Computational geometrically nonlinear vibration analysis of uncertain mistuned bladed disks

Evangéline Capiez-Lernout, Christian Soize, M. Mbaye

Proceedings of ASME Turbo Expo 2014: Turbine Technical Conference and Exposition
GT2014

June 16-20, 2014, Düsseldorf, Germany

GT2014-25072

COMPUTATIONAL GEOMETRICALLY NONLINEAR VIBRATION ANALYSIS OF UNCERTAIN MISTUNED BLADED DISKS

Evangéline Capiez-Lernout
Université Paris-Est
Modélisation et Simulation
Multi-Echelle
MSME UMR 8208 CNRS
77454 Marne-la-Vallée Cedex 02
France
evangeline.capiez-lernout@u-pem.fr

Christian Soize
Université Paris-Est
Modélisation et Simulation
Multi-Echelle
MSME UMR 8208 CNRS
77454 Marne-la-Vallée Cedex 02
France
christian.soize@u-pem.fr

Moustapha Mbaye
Turbomeca - Safran Group
64511 Bordes, France
moustapha.mbaye@turbomeca.fr

ABSTRACT

The recent improvements in turbomachinery design requires the analysis of exceptional operating regime of bladed disks corresponding to geometrical nonlinear effects induced by the large displacements/deformations. In addition, the random nature of the mistuning has also to be modeled. First, a mean nonlinear reduced-order model of the tuned bladed disk is explicitly constructed in the context of the finite element method. The investigation is then devoted to the modeling of the mistuning through the nonparametric probabilistic approach extended to the nonlinear geometric context. The stochastic nonlinear equations are solved in the time domain using the Monte Carlo numerical simulation coupled with advanced arc-length methods adapted to high nonlinear response levels. Finally, the methodology is applied through a numerical example of a bladed disk and a nonlinear analysis is performed in both time and frequency domain.

NOMENCLATURE

$g(t)$ Time domain of the load
$\hat{g}(\omega)$ Frequency domain of the load
j_0, k_0 Blade number
n number of degrees of freedom
n_t Number of time steps
r Load rate
$s\Delta\omega$ Centered frequency of $\mathbb{B}_s$
t_{ini} Initial instant of integration
$v(t)$ Time domain observation (mean NL-ROM)
$w(\omega)$ Frequency domain observation (mean NL-ROM)
N Order of the cyclic symmetry
P Dimension of the NL-ROM
T Total duration time
$V(t)$ Time domain observation (stochastic NL-ROM)
V_∞ Time domain observation (stochastic NL-ROM)
$W(\omega)$ Frequency domain observation (stochastic NL-ROM)
$Y(\omega)$ Magnification factor (stochastic NL-ROM)
$\delta\nu$ Frequency resolution
δ Dispersion parameter
ν Frequency (Hz)
ω_{min} Lower bound of $\mathbb{B}_s$
ω Pulsation $(rad.s^{-1})$
$\Delta\omega$ Width of $\mathbb{B}_s$
Ω Angular speed (rotational motion)
$\mathbb{B}$ Frequency band of analysis
$\mathbb{B}_s$ Frequency band of excitation
$\mathbb{R}$ Real vector space
$\boldsymbol{\alpha}$ Spatial discretization of the load
$\mathbf{f}$ External load vector
$\mathbf{f}^{NL}(\mathbf{u})$ Nonlinear restoring force
$\mathbf{q}$ vector of the generalized coordinates (mean NL-ROM)

$\mathbf{u}$ Displacement vector (mean computational model)
$\tilde{\mathbf{u}}$ Observation vector (mean NL-ROM)
$[A]$ Finite element matrices (Roman capital letters)
$[\Phi]$ Modal matrix

INTRODUCTION

There are many aspects to be taken into consideration when dealing with turbomachinery bladed disks. The predictive computational models are more and more sophisticated, including the modeling of complex phenomena occurring in such structures. It is well known, that the manufacturing tolerances, the dispersion of materials, which arouses in bladed disks structures create uncertainties on the geometry, on the boundary conditions and on the material properties, which breaks the natural cyclic symmetry of such structures. The main consequence results in strong vibrations combined to spatial localization in the dynamic forced response of the blades [1]. The random character of such phenomenon referred to as mistuning requires the use of adapted probabilistic model of uncertainties in the computational models [2–5]. Another essential aspect to be taken into account concerns the modeling of the different nonlinearity sources such as nonlinear contact interfaces [6–8] or geometrically nonlinear effects [9–12]. At the same time, the progression of the computational capabilities, which includes the possibility of using parallel computations, has been a motivation to develop computational strategies adapted to large finite element model of industrial bladed disks. Various researches concerning reduced-order modeling techniques adapted to the mistuned linear analysis of bladed disks [2, 13] have been used for robust design optimization purpose [14–16]. Adapted reduced-order techniques have also been proposed in [17, 18] for the nonlinear dynamical analysis of turbomachines.

In the present case, we are interested in the geometrically nonlinear analysis of mistuned bladed disks. The recent improvements in turbomachinery design requires the analysis of exceptional operating regime of bladed disks for which large displacements/deformations can occur. The case of severe loading is investigated in the context of elasto-dynamics. Such situation is equivalent to nearly unstable cases induced by aerodynamic coupling yielding flutter and thus very low damping levels. In such case, the linearized elasto-dynamic theory can not be used anymore because the geometrically nonlinear effects induced by the large deformations and the large displacements are very strong and need to be taken into account in the modeling.

The methodology is developed in the context of large finite element computational model of bladed disks, requiring the construction of adapted nonlinear reduced-order computational models (NL-ROM). The developments of such NL-ROM requires the selection of an appropriate deterministic basis for the representation of the nonlinear dynamic response. More generally, this projection basis can be obtained by using the proper-orthogonal decomposition method or by an eigenvalue analysis. A mixed formulation combining these two approaches has been proposed in [19]. Strategies based on the selective choice of the most appropriate basis are reviewed in [20]. The parameters of the NL-ROM of the tuned structure can then be either deduced using the STEP procedure (which is based on the smart non-intrusive use of standard commercial finite element codes) [20–22] or from explicit construction as shown in [23] in the context of three-dimensional solid finite elements. Once the NL-ROM of the tuned bladed disk is established, uncertainties can be implemented through the nonparametric framework [24, 25], which has been extended in the nonlinear geometric case [22]. Such probabilistic approach is able to simultaneously capture both system-parameter uncertainties and model uncertainties. It relies on the dedicated construction of a probability model related to the tuned NL-ROM operators, using the maximum entropy principle (MaxEnt).

The paper is organized as follows. Section 1 gives a complete description of the computational methodology and of its numerical aspects allowing the nonlinear dynamic analysis of mistuned bladed-diks to be performed. The mean NL-ROM corresponding to the tuned structure is explicitly constructed following the approach presented in [23]. Once the mistuning is modeled through the nonparametric probabilistic approach, the numerical strategy concerning the resolution of the set of nonlinear coupled differential equations is discussed. Section 2 is devoted to a numerical example, for which the geometrically nonlinear effects are analyzed and quantified in both tuned and mistuned cases.

METHODOLOGY

This Section is devoted to the construction of a methodology for the nonlinear mistuning analysis occurring in rotating bladed disks structures. In the present research, the bladed disks under consideration are assumed (1) to be made up of a linear elastic material and (2) to undergo large displacements and large deformations inducing geometrical nonlinearities.

Nonlinear dynamics of a tuned bladed disk

The tuned bladed disk structure has an $N-$order cyclic symmetry. Thus, the geometrical domain, the material constitutive equations and the boundary conditions related to the generating sector are invariant under the $\frac{2\pi}{N}$ rotation around its axis of symmetry. Moreover, the bladed disk undergoes a rotational motion around the axis of symmetry with constant angular speed Ω. By choosing a total Lagrangian formulation, the dynamical equations are expressed in the rotating frame of an equilibrium configuration considered as a prestressed static configuration.

The mean (or nominal) computational model of the tuned bladed disk, which is constructed by the Finite Element Method

(FEM) is written as [26]:

$$[M]\,\ddot{\mathbf{u}} + ([C(\Omega)] + [D])\dot{\mathbf{u}} + [K^1(\Omega)]\mathbf{u} + \mathbf{f}^{NL}(\mathbf{u}) = \mathbf{f} \quad ,$$
$$[K^1(\Omega)] = [K_e] + [K_g] + [K_c(\Omega)] \quad , \qquad (1)$$

in which the $\mathbb{R}^n$-vector $\mathbf{f}$ is the external load representing for instance the unsteady pressures applied to the blades, and where the $\mathbb{R}^n$-vector $\mathbf{u}$ corresponds to the finite element discretization of the unknown displacement field. In Eq. (1), the matrices $[M]$, $[D]$, $[K_g]$ and $[K_e]$ are the mass, damping, geometrical stiffness and elastic stiffness real matrices with positive definiteness property. The rotational effects are taken into account through the gyroscopic coupling matrix $[C(\Omega)]$ and the centrifugal stiffness matrix $[K_c(\Omega)]$, which have respectively antisymmetry property and negative definiteness property. It should be noted that all these matrices are also N-block circulant matrices [27] since the structure has an N-order cyclic symmetry. The geometrical nonlinearities effects are taken into account through the $\mathbb{R}^n$-vector $\mathbf{f}^{NL}(\mathbf{u})$ which includes the exact and complete quadratic and cubic terms given by the three-dimensional nonlinear geometric elasticity. Furthermore, the centrifugal effects are assumed to be sufficiently small so that the linear stiffness matrix $[K^1(\Omega)]$ is positive definite, yielding only stable dynamical systems to be considered.

In the present case, the presence of the geometric nonlinearity naturally yields the nonlinear equations to be solved in the time domain, the frequency content of the nonlinear response being *a posteriori* analyzed by Fourier transform. Concerning the external load, a usual harmonic excitation would be inappropriate because the nonlinear equations should be solved for each harmonic excitation considered. The external load is then defined in the time domain corresponding to a uniform sweep of a chosen frequency band of excitation. Let $\widetilde{\mathbb{B}}_s = -\mathbb{B}_s \cup \mathbb{B}_s$ be the frequency band of excitation with central frequency $s\Delta\omega$ and bandwidth $\Delta\omega$ defined by $\mathbb{B}_s = [(s-1/2)\Delta\omega, (s+1/2)\Delta\omega]$. The external load is written as

$$\mathbf{f}(t) = f_0\, g(t)\, \boldsymbol{\alpha} \quad , \qquad (2)$$

in which f_0 is a coefficient characterizing the global load intensity, and where $\boldsymbol{\alpha}$ is an $\mathbb{R}^n-$vector corresponding to the spatial discretization of the load. In Eq. (2), the function $g(t)$ is chosen as $g(t) = \dfrac{\Delta\omega}{\pi} sinc_\pi(\dfrac{t\Delta\omega}{2\pi}) cos(s\Delta\omega t)$, where $x \mapsto sinc_\pi(x)$ is the special function defined by $sinc_\pi(x) = sin(\pi x)/(\pi x)$. It should be noted that all the frequencies of the frequency band of excitation are simultaneously excited so that only one nonlinear time-domain analysis is carried out. With such time-domain excitation, a forced-response problem is considered and not a time evolution problem with initial conditions. The considered forced-response problem is thus approximated by an equivalent time-evolution problem with zero initial conditions over a finite time interval, which includes almost all of the signal energy of the excitation.

The use of the cyclic symmetry property by decomposing the nonlinear response according to its harmonic components is not considered in the present case because all the harmonic components are coupled through the geometric nonlinearity and does not allow the problem on a single rotor sector to be solved. Moreover, the full computation of the nonlinear solution of Eq. (1) can not be reasonably performed when dealing with realistic models of bladed disks corresponding to a large number of DOF. More specifically, large dimensional computational models require to develop reduced-order model strategies adapted to this geometric nonlinear context (see [19, 21, 23] and [20] for a complete overview). Let be a given vector basis represented by the $(n \times P)$ real matrix $[\Phi]$. The nonlinear response $\mathbf{u}$ is expanded as

$$\mathbf{u} = [\Phi]\,\mathbf{q} \quad , \qquad (3)$$

in which $\mathbf{q}$ is the $\mathbb{R}^P$-vector of the generalized coordinates. Replacing Eq. (3) in Eq. (1) yields a nonlinear reduced set of P coupled differential equations for which all linear, quadratic and cubic terms have to be known. In the present research, the construction of the operators of such mean NL-ROM is explicitly carried out in the context of the three-dimensional finite element method. The finite elements are isoparametric solid finite elements with 8 nodes using a numerical integration with 8 Gauss integration points. The elementary internal forces projected on the chosen vector basis are numerically constructed for each finite element before performing its assembly and computing all linear and nonlinear reduced operators. The detailed procedure, which also uses the symmetry properties of the linear and nonlinear reduced-operators combined with distributed computations, can be found in [23]. It should be noted that each type of reduced operator is separately modeled, keeping open the possibility of implementing uncertainties issued from independent physical sources.

Nonlinear dynamics of a mistuned bladed disk

The random nature of the mistuning is then considered by implementing the nonparametric probabilistic approach, which presents the ability to include both system-parameter uncertainties and model uncertainties (see [25] for a complete review on the subject). It consists in replacing the operators of the mean NL-ROM by random operators, whose probability distribution is derived from the maximum entropy principle. In the present case, the mass, damping, geometrical stiffness and the opposite of the centrifugal stiffness are positive definite operators whose probability model is constructed from the usual nonparametric

probabilistic approach [24]. The linear elastic, quadratic and cubic stiffness reduced operators are reshaped in a positive-definite operator as shown in [22], which allows the nonparametric probabilistic theory to be extended to the geometric nonlinear case. The stochastic model of the gyroscopic coupling is constructed with a similar method as proposed in [28] for the aero-elastic coupling. The dispersion of each random operator is then characterized by one scalar parameter. Consequently, the mistuning level of the bladed disk is entirely controlled by the $\mathbb{R}^6$-vector $\delta = (\delta_M, \delta_D, \delta_C, \delta_{K_g}, \delta_{K_c}, \delta_K)$.

Numerical computations

The solution of the stochastic NL-ROM is calculated using the Monte Carlo numerical simulation. For each realization, a set of P nonlinear coupled differential equations is considered and solved with the Newmark method, for which the averaging acceleration scheme, known to be unconditionally stable is used. With this solver, a set of nonlinear equations whose solution is denoted by the $\mathbb{R}^P$-vector q has to be solved at each sampling time. Such computation is mainly addressed by the fixed point method because the iterative scheme does not require the evaluation of the tangential stiffness matrix. Nevertheless, when the algorithm does not converge, it is replaced by the Crisfield arc-length method [29]. Such algorithm introduces an additional scalar unknown μ that multiplies the right-hand side of the nonlinear equation. It is solved step by step, each incremental step being characterized by a given arc-length. For a given step, an iterative scheme requiring one evaluation of the tangential stiffness matrix allows a solution (q, μ) to be computed. An adaptive arc-length, depending on the number of iterations necessary to obtain the convergence of the preceding increment is also implemented. Furthermore, since parameter μ has to be controlled to be equal to 1, the state of the algorithm corresponding to the preceding increment has to be stored. Even if the procedure is time consuming, its main advantage concerns its capability of capturing high non-linear mechanical behaviors.

NUMERICAL EXAMPLE

Description of the mean computational model

The structure under consideration is a bladed disk constituted of a disk and 24 blades. The disk is made of a homogeneous and isotropic material with constant thickness $0.005m$, inner radius $0.035m$, outer radius $0.1m$, mass density $7860 Kg.m^{-3}$, Poisson ratio 0.25 and Young modulus $2 \times 10^{11} N.m^{-2}$. Fixed conditions are applied along the internal boundary defined by the inner radius. Each blade is made of the same homogeneous and isotropic material as the disk one with length $0.07\,m$, width $0.0085m$, linear decreasing thickness from $0.005\,m$ to $0.001\,m$. The structure is in rotation around its revolution axis with a constant angular speed $\Omega = 30\,000\,rpm$. Since the dynamic analysis is carried out in the rotating frame of the structure, the rigid-body motion due to the rotation of the structure corresponds to a fixed boundary condition at the inner radius of the structure. A damping model is added for the bladed disk, corresponding to a hysteretic model with a mean loss factor 2×10^{-7}, which corresponds to a modal damping around 0.001 for the low frequency band of interest defined by $\mathbb{B} = [0\,,\,3\,900]\,Hz$.

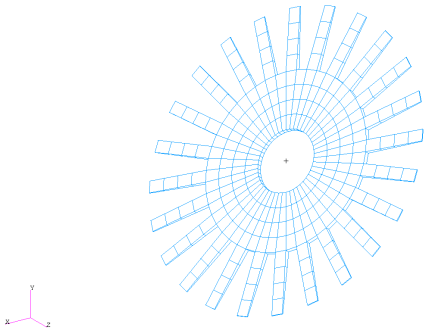

FIGURE 1. FINITE ELEMENT MESH.

TABLE 1. DATA FOR THE FE MODEL

	FE	Nodes	DOF
Sector	12	46	138
Bladed disk	288	864	2592

The full finite element model, shown in Fig.1, is built with $288\,8-$nodes solid finite elements and is thus constituted of $2\,592$ degrees of freedom (see Table 1 for the detailed data related to the mesh of the structure).

Nonlinear analysis of the tuned bladed disk

Tuned linear eigenfrequencies The natural eigenfrequencies of the linear tuned bladed disk are calculated first by using the cyclic symmetry property of the structure [30,31]. Figure 2 displays these eigenfrequencies as a function of its circumferential wave number.

Description of the external load Concerning the modeling of the external load according to Eq.(2), the frequency band of excitation is chosen with regard to Fig.2 such that $\mathbb{B}_s = [3000\,,\,3207]\,Hz$, which corresponds to $s = 15$ and $\Delta\omega = 1\,300\,rad.s^{-1}$. The spatial distribution of the load is only concerned with point excitations located at the end of each blade along the transverse direction. Vector α characterizing the spa-

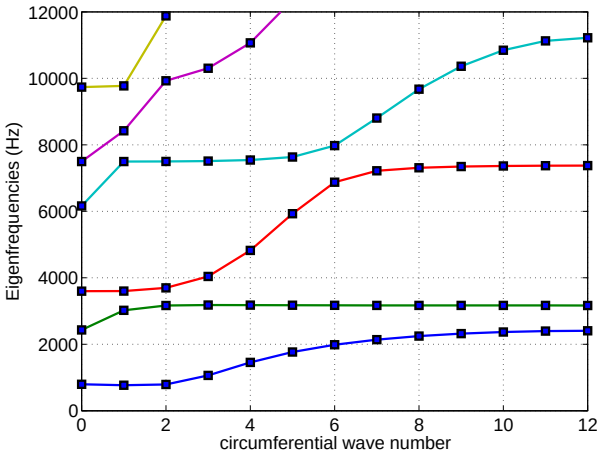

FIGURE 2. NATURAL FREQUENCIES WITH RESPECT TO CIRCUMFERENTIAL WAVE NUMBER

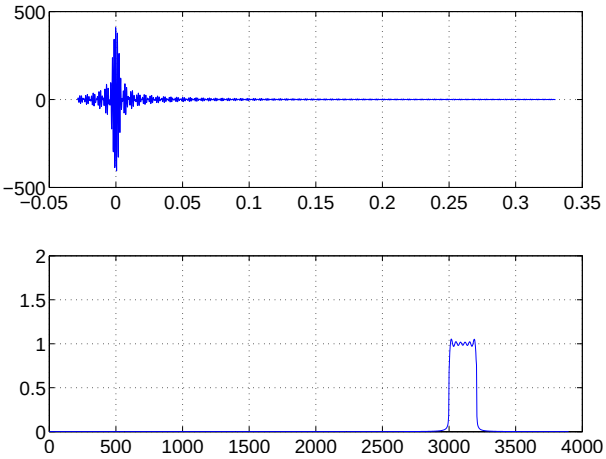

FIGURE 3. REPRESENTATION OF THE EXTERNAL LOAD IN THE TIME AND FREQUENCY DOMAIN: GRAPH OF $t \mapsto g(t)$ (UPPER GRAPH) and $\nu \mapsto \hat{g}(2\pi\nu)$ (LOWER GRAPH).

tial distribution from blade to blade has then 24 non zeros components, which are uniformly distributed from blade to blade. In that case when the tuned linear case is considered, there are contributions on all the circumferential wave number. The external load is thus considered as a function of f_0. Concerning the numerical sampling, the initial instant of integration t_{ini} and the total time duration T are chosen according to [32] such that $t_{ini} = -0.029\,s$ (corresponding to a zero value of function $g(t)$) and $T = 0.36\,s$. Given $\mathbb{B}$ combined with the Shannon theorem yields the number n_t of time steps to be $n_t = 2800$. The frequency resolution is then $\delta\nu = 2.78\,Hz$. Let $\hat{g}(\omega)$ be the Fourier transform of function $g(t)$. Figure 3 shows the graphs $t \mapsto g(t)$ and $\nu \mapsto \hat{g}(2\pi\nu)$, in which $\nu = \dfrac{\omega}{2\pi}$.

Convergence analysis of the mean NL-ROM Concerning the choice of the vector basis for the construction of the mean NL-ROM, a strategy would consist in using the proper orthogonal decomposition method (POD). This would require the knowledge of the full reference solution, which is practically not possible to get, when considering realistic bladed disk models involving large number of degrees of freedom (DOF). In the present case, the nonlinear equations are solved in the subspace spanned by the usual linear basis constituted of the P modal shapes related to the first increasing natural eigenfrequencies, according to [23]. Zero initial conditions are used. The observation is given by the $\mathbb{R}^N$-vector $\tilde{\mathbf{u}}^P$ corresponding to the out-plane dof located at the end of each blade. An incremental convergence analysis is carried out for a maximum load of $f_0||\boldsymbol{\alpha}|| = 3.512\,N$, corresponding to an high rate of geometrical nonlinearity. Such high loading can be interpreted as equivalent to a situation for which the damping of the bladed disk structure would reach very small values. Such extreme situations are realistic when flutter occurs and yields nearly unstable situations. Let $Conv(P)$ be the function defined by

$$Conv(P) = \int_{t_{ini}}^{t_{ini}+T} ||\tilde{\mathbf{u}}^P(t)||^2\,dt \quad . \tag{4}$$

Figure 4 displays the graph $P \mapsto Conv(P)/Conv(150)$ in a logarithmic scale. It can be seen that $P = 90$ yields a reasonable convergence. From now on, the calculations will be carried out for $P = 100$.

Nonlinear time domain analysis From now on, the converged solution corresponding to the observation issued from the mean NL-ROM is denoted by $\tilde{\mathbf{u}}(t)$. For clarity, when confusion is possible, superscripts ^{LIN} and ^{NONLIN} will be added for distinguishing the linear case from the geometric nonlinear one. Let be the load rate such that $r = 100\%$ when intensity load is $f_0||\boldsymbol{\alpha}|| = 3.512\,N$.

The intensity loads considered are then described by $r\,f_0||\boldsymbol{\alpha}||$ with $r \in]0,1]$. Being interested in the blade yielding the highest vibration amplitude, let $j_0 = \arg\max_j \left(\max_t \tilde{u}_j^{NONLIN}(t)\right)$ calculated for a load rate $r = 100\%$. The observation $v(t)$ corresponding to the selected blade out-plane displacement is defined by $v(t) = \tilde{u}_{j_0}(t)$. Figures 5 and 6 display the graphs $t \mapsto v^{LIN}(t)$ (upper graph) and $t \mapsto v^{NONLIN}(t)$ (lower graph) for load rates $r = 20\%$ and $r = 100\%$ corresponding to significant levels and very high levels of geometric nonlinear effects. On these two figures, it is seen that the geometric nonlinearities induce a blade stiffening

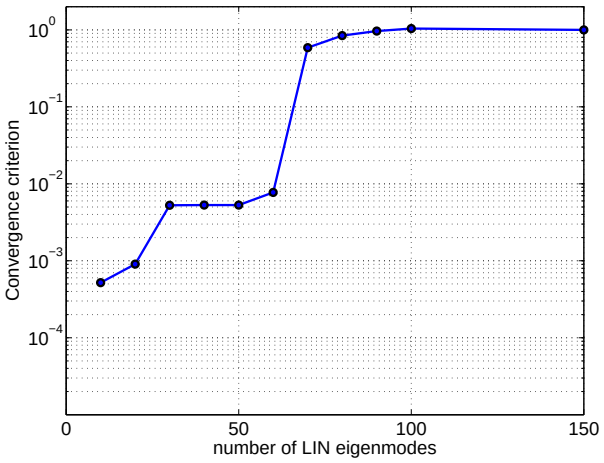

FIGURE 4. CONVERGENCE ANALYSIS OF THE NL-ROM OF THE TUNED BLADED DISK: GRAPH OF FUNCTION $P \mapsto Conv(P)$

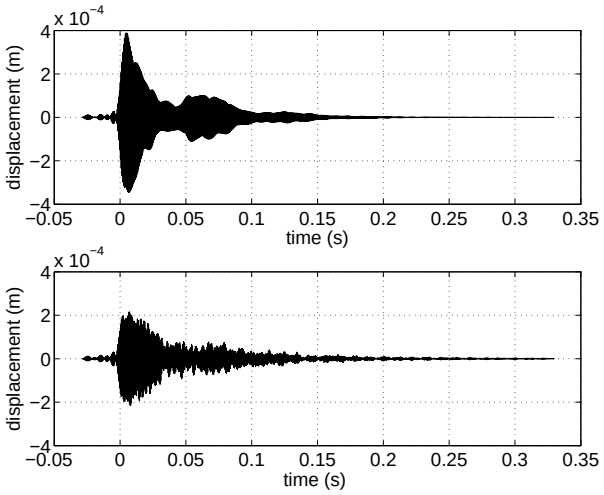

FIGURE 5. TIME DOMAIN OBSERVATION $t \mapsto v(t)$ RELATED TO THE LINEAR (UPPER GRAPH) AND NONLINEAR (LOWER GRAPH) CASES FOR $r = 20\%$

characterized by a reduction of the vibration amplitudes of the blades with respect to the linear case. This stiffening is also combined with a strong irregularity of the blade response shape over time, which shows an enrichment of the frequency content, which has to be quantified.

Nonlinear frequency domain analysis Let $k_0 = \arg\max_j \left(\max_{\omega\in\mathbb{B}} \widehat{\widetilde{u}}_j^{NONLIN}(\omega)\right)$ for which $\widehat{\widetilde{u}}_j^{NONLIN}(\omega)$ is the Fourier transform of $\widetilde{u}_j^{NONLIN}(t)$ calculated for $r = 100\%$.

In the frequency domain, the observation $w(\omega)$ corresponding to the selected blade out-plane displacement is defined by $w(\omega) = \widehat{\widetilde{u}}_{k_0}(\omega)$. Figures 7 and 8 display the graphs $\nu \mapsto w^{LIN}(2\pi\nu)$ (upper graph) and $\nu \mapsto w^{NONLIN}(2\pi\nu)$ (lower graph) for load rates $r = 20\%$ and $r = 100\%$. As expected, it can be seen that the frequency content of the blade response issued from the linear NL-ROM coincides with $\mathbb{B}_s$. The coupling issued from the strong nonlinear geometric effects is characterized through secondary response peaks, whose frequency content en-

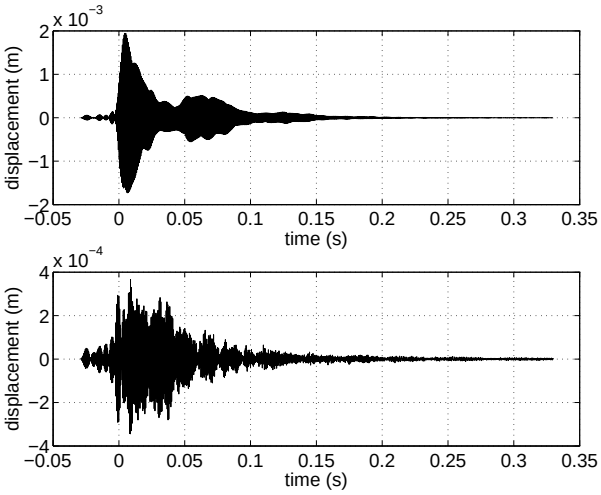

FIGURE 6. TIME DOMAIN OBSERVATION $t \mapsto v(t)$ RELATED TO THE LINEAR (UPPER GRAPH) AND NONLINEAR (LOWER GRAPH) CASES FOR $r = 100\%$

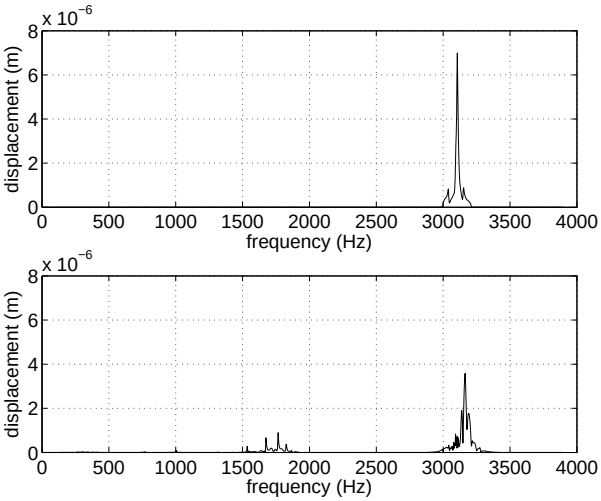

FIGURE 7. FREQUENCY DOMAIN OBSERVATION $\nu \mapsto w(2\pi\nu)$ RELATED TO THE LINEAR (UPPER GRAPH) AND NONLINEAR (LOWER GRAPH) CASES FOR $r = 20\%$

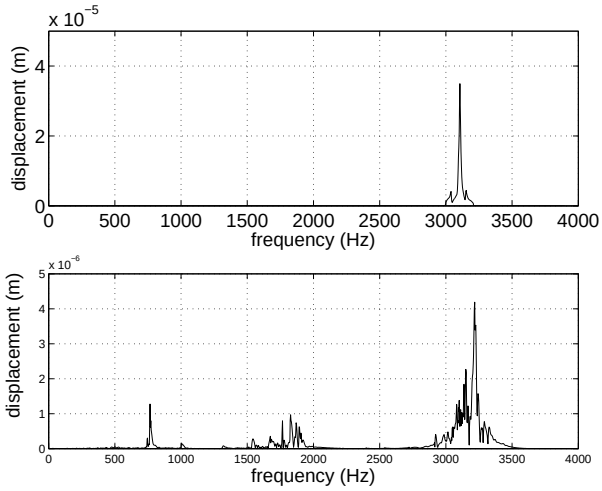

FIGURE 8. FREQUENCY DOMAIN OBSERVATION $v \mapsto w(2\pi v)$ RELATED TO THE LINEAR (UPPER GRAPH) AND NONLINEAR (LOWER GRAPH) CASES FOR $r = 100\%$

larges with increasing load rate. It should be noted that there also exist higher frequencies excited through this nonlinearity which are not observed in the chosen band of analysis $\mathbb{B}$. As observed on the graphs, the amplitude levels from linear and high nonlinear cases are drastically different.

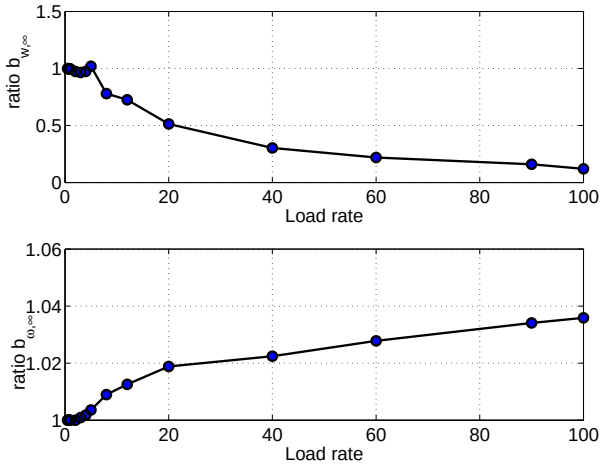

FIGURE 9. SENSITIVITY ANALYSIS WITH RESPECT TO THE LOAD RATE;

A sensitivity analysis is then conducted in order to quantify these geometric nonlinear effects. Let $b_{w,\infty}$ and $b_{\omega,\infty}$ be the amplitude ratio and frequency ratio defined by

$$b_{w,\infty} = \frac{\max_{\omega\in\mathbb{B}} w^{NONLIN}(\omega)}{\max_{\omega\in\mathbb{B}} w^{LIN}(\omega)}$$
$$b_{\omega,\infty} = \frac{\arg\max_{\omega\in\mathbb{B}} w^{NONLIN}(\omega)}{\arg\max_{\omega\in\mathbb{B}} w^{LIN}(\omega)} \qquad (5)$$

Figure 9 displays the graphs $r \mapsto b_{w,\infty}(r)$ (upper graph) and $r \mapsto b_{\omega,\infty}(r)$ (lower graph). Such graphs is able to show if the analyzed response belongs or not to the nonlinear domain of analysis. When the values of observations $b_{w,\infty}$ and $b_{\omega,\infty}$ are different from 1, the domain of analysis is nonlinear. It can be seen that geometric nonlinear effects occurs from $r = 2\%$. A quick decrease in amplitude is combined to a moderate shift of the main response peak when r increases.

Nonlinear analysis of the mistuned bladed disk

Mistuning implementation The mean NL-ROM used above is re-used for considering the mistuned bladed disk. The stochastic NL-ROM is defined from the mean NL-ROM by replacing the operators of the mean NL-ROM by random operators according to the nonparametric probabilistic theory [25]. Since the NL-ROM is constructed by modal analysis without substructuring techniques, the uncertainties are not considered to be independent from one blade to another one, which restricts the analysis to the class of integrated bladed disks, manufactured from a unique solid piece of material. In order to simplify the analysis, the extension being straightforward, only the linear elastic part is considered to be uncertain. In that case, the reduced positive-definite operator $[\Phi]^T [K_e] [\Phi]$, which can be written such that $[\Phi]^T [K_e] [\Phi] = [L]^T [L]$ is replaced by the random operator $[L]^T [\mathbf{G}(\delta)] [L]$, in which $[\mathbf{G}(\delta)]$ is a random operator whose probability distribution is entirely described in [25]. The dispersion parameter δ is then a scalar parameter. According to the nonparametric probabilistic theory, it allows the uncertainty level of the stochastic NL-ROM to be controlled. In the present case, numerical simulations are carried out for dispersion level $\delta = 0.02$ (small mistuning) and $\delta = 0.1$ (moderate mistuning) and with $r = 100\%$.

Nonlinear time domain analysis The nonlinear mistuning analysis is first considered in the time domain. For fixed t, observation $v(t)$ is replaced by the random variable $V(t)$. The numerical simulations are carried out with $n_s = 1024$ Monte Carlo realizations, which is sufficient to get the convergence of $\mathbb{E}\{V^2(t)\}$, in which $\mathbb{E}$ is the mathematical expectation. Let V_∞ be the random variable defined by

$$V_\infty = \max_{t\in[t_{ini};t_{ini}+T]} V(t) \quad . \qquad (6)$$

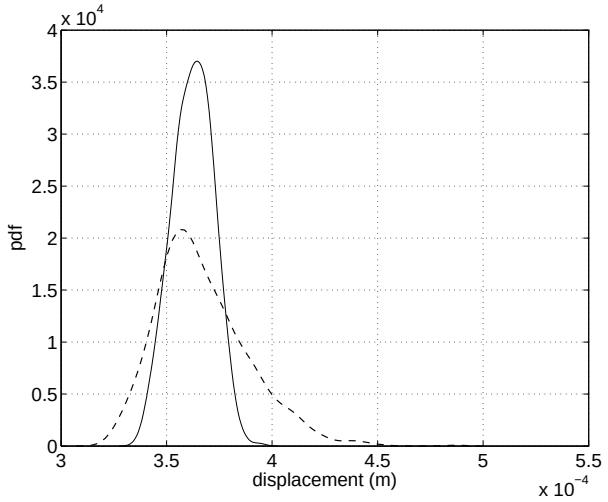

FIGURE 10. PROBABILITY DISTRIBUTION FUNCTION OF V_∞ FOR $\delta = 0.02$ (SOLID LINE) AND $\delta = 0.1$ (DASHED LINE)

Figure10 displays the graph of the probability distribution function $v \mapsto p_{V_\infty^{NONLIN}}(v)$, which is computed using the kernel density estimation [33]. It has to be compared with the value $v = 3.665 \times 10^{-4} m$ related to the nonlinear analysis of the tuned bladed disk (see Fig.6). When δ increases from 0.02 to 0.1, the coefficient of variation of the observation is doubled from 0.027 to 0.059, yielding a broader range taken by the Monte Carlo realizations. Moreover, a significant loss of symmetry of the probability distribution function, quantified by a variation of the skewness from -0.07 to 0.86 can be seen. It is characterized by a shift of the support to higher values, yielding a few realizations of the observation to be increased of 40% with respect to the nonlinear tuned case.

Nonlinear frequency domain analysis A Fourier transform is then conducted in order to perform the nonlinear analysis in the frequency domain. For fixed ω, let $Y(\omega)$ be the random dynamic magnification factor defined by

$$Y(\omega) = \frac{W(\omega)}{\max_{\omega \in \mathbb{B}} w(\omega)} \quad , \tag{7}$$

in which $W(\omega)$ is the random variable similar to observation $w(\omega)$ in the nonlinear tuned case. It should be noted that $Y(\omega)$ is a normalized random quantity and that the amplitude levels between the geometric nonlinear case and the linear case are about an order smaller.

Figures 11 and 12 display the graphs of the confidence region of $v \mapsto Y^{LIN}(2\pi v)$ calculated with a 95% probability level for $r = 100\%$, $\delta = 0.01$ and $\delta = 0.2$. Figures 13 and 14 display

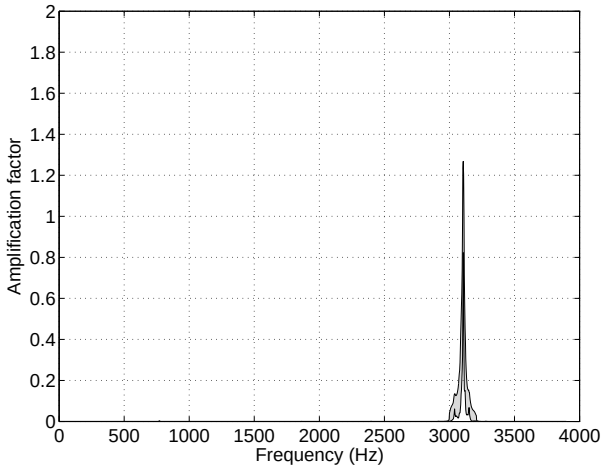

FIGURE 11. CONFIDENCE REGION OF THE DYNAMIC MAGNIFICATION FACTOR $v \mapsto Y^{LIN}(2\pi v)$ FOR THE LINEAR CASE WITH $\delta = 0.02$.

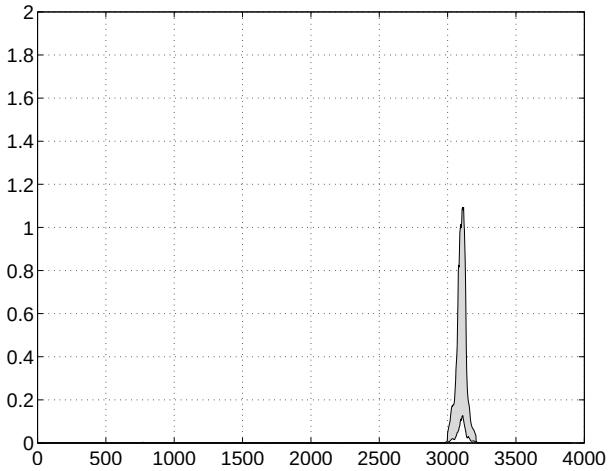

FIGURE 12. CONFIDENCE REGION OF THE DYNAMIC MAGNIFICATION FACTOR $v \mapsto Y^{LIN}(2\pi v)$ FOR THE LINEAR CASE WITH $\delta = 0.1$.

the similar graphs for random observation $v \mapsto Y^{NONLIN}(2\pi v)$. Comparing the linear case with the nonlinear case shows that the effects of uncertainties increase with the geometric nonlinearity. For fixed δ, it can be seen on these figures that the confidence region related to the peak located around $\mathbb{B}_s$ is very sensitive to uncertainties, when considering the geometric nonlinear case, yielding a broad confidence region and some realizations with 40% (or 30%) amplification effect with $\delta = 0.02$ (or $\delta = 0.1$). A small softening effect is also observed with a 0.5% decreasing shift of the frequency resonance. The uncertainties are also propagated on the secondary peaks excited through the geomet-

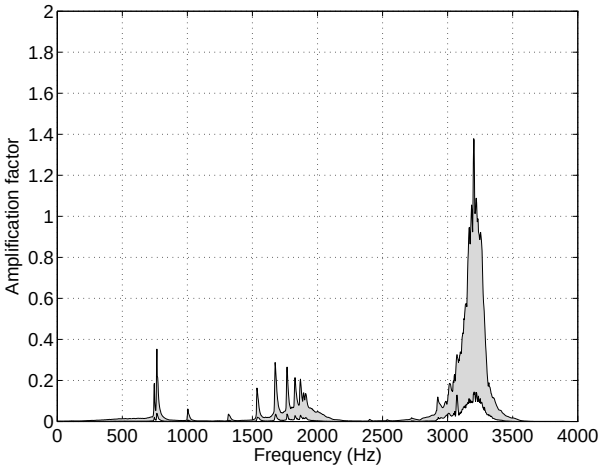

FIGURE 13. CONFIDENCE REGION OF THE DYNAMIC MAGNIFICATION FACTOR $\nu \mapsto Y^{NONLIN}(2\pi\nu)$ FOR THE GEOMETRIC NONLINEAR CASE WITH $\delta = 0.02$

ric nonlinearities. Although the amplitudes of these peaks are marginal compared to the main vibration peak, the sensitivity to uncertainties is larger.

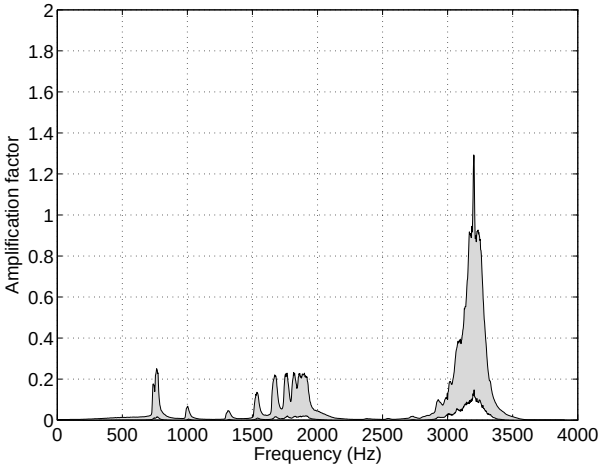

FIGURE 14. CONFIDENCE REGION OF THE DYNAMIC MAGNIFICATION FACTOR $\nu \mapsto Y^{NONLIN}(2\pi\nu)$ FOR THE GEOMETRIC NONLINEAR CASE WITH $\delta = 0.1$

CONCLUSION

The paper has presented an analysis of the geometrical nonlinear effects of uncertain mistuned bladed disk, corresponding to the particular case for which aerodynamic coupling yields flutter, that is to say nearly unstable situations with very low damping, which is represented by an high loading level. Firstly, a nonlinear dynamic analysis of the tuned bladed disk is proposed through the construction of a NL-ROM. The effects of the geometric nonlinearities, corresponding to a quick stiffening of the structure when reaching a critical level of loading, are quantified in both time domain and frequency domain. The dynamical response of the blades is also investigated outside the frequency domain of excitation. The linear response has its energy concentrated in the frequency domain of excitation whereas the nonlinear response is spread over a larger frequency domain. Then, the nonlinear analysis of the mistuned structure is proposed in the context of integrally bladed disks, assuming the uncertainties from one blade to another one to be dependent. Compared to the linear mistuned case, the nonlinear mistuned response predictions yield low vibration amplitudes. Nevertheless, for a given mistuning rate, the nonlinear mistuned response predictions display broader confidence regions and are much more sensitive to uncertainties. Such decrease of robustness with respect to uncertainties propagates quickly in the whole frequency band of analysis. This yields a complex vibratory situation, giving rise to frequency ranges for which secondary resonances appear with large confidence regions.

ACKNOWLEDGMENT

This work was supported by the DGA (French defence procurement agency) in the context of the TURBODYNA project (project number ANR-13-ASTR-0008-01) related to the ANR ASTRID research program (specific support scheme for research works and innovation defence).

REFERENCES

[1] Wei, S.-T., and Pierre, C., 1988. "Localization phenomena in mistuned assemblies with cyclic symmetry part ii: Forced vibrations". *Journal of Vibration, Acoustics Stress and Reliability in Design,* ***110***(4), pp. 439–449.

[2] Bladh, R., Castanier, M.-P., and Pierre, C., 2001. "Component-mode-based reduced order modeling techniques for mistuned bladed disks - part i: Theoretical models". *ASME Journal of Engineering for Gas Turbines and Power,* ***123***(1), pp. 89–99.

[3] Rivas-Guerra, A.-J., Mignolet, M.-P., and Delor, J.-P., 2001. "Identification of mistuning characteristics of bladed disks from free response data - part ii". *ASME Journal of Engineering for Gas Turbines and Power,* ***123***(2), pp. 404–411.

[4] Mignolet, M.-P., and Soize, C., 2008. "Nonparametric stochastic modeling of linear systems with prescribed vari-

ance of several natural frequencies". *Probabilistic Engineering Mechanics,* ***23***(2-3), pp. 267–278.

[5] Capiez-Lernout, E., and Soize, C., 2004. "Nonparametric modeling of random uncertainties for dynamic response of mistuned bladed disks". *ASME Journal of Engineering for Gas Turbines and Power,* ***126***(3), pp. 610–618.

[6] Petrov, E.-P., 2009. "Analysis of sensitivity and robustness of forced response for nonlinear dynamic structures". *Mechanical Systems and Signal Processing,* ***23***(1), pp. 68–86.

[7] Petrov, E.-P., 2012. "Analysis of flutter-induced limit cycle oscillations in gas-turbine structures with friction, gap, and other nonlinear contact interfaces". *Journal of Turbomachinery,* ***134***(6).

[8] Laxalde, D., Thouverez, F., Sinou, J.-J., and Lombard, J.-P., 2007. "Qualitative analysis of forced response of blisks with friction ring dampers". *European Journal of Mechanics, A/Solids,* ***26***(4), pp. 676–687.

[9] Vakakis, A., 1992. "Dynamics of a nonlinear periodic structure with cyclic symmetry". *Acta Mechanica,* ***95***(1-4), pp. 197–226.

[10] Sarrouy, E., Grolet, A., and Thouverez, F., 2011. "Global and bifurcation analysis of a structure with cyclic symmetry". *International Journal of Non-Linear Mechanics,* ***46***(5), pp. 727–737.

[11] Grolet, A., and Thouverez, F., 2011. "Vibration analysis of a nonlinear system with cyclic symmetry". *Journal of Engineering for Gas Turbines and Power,* ***133***(2).

[12] Grolet, A., and Thouverez, F., 2012. "Free and forced vibration analysis of a nonlinear system with cyclic symmetry: Application to a simplified model". *Journal of Sound and Vibration,* ***331***(12), pp. 2911–2928.

[13] Yang, M.-T., and Griffin, J., 2001. "A reduced-order model of mistuning using a subset of nominal modes". *ASME Journal of Engineering for Gas Turbines and Power,* ***123***(3), October, pp. 893–900.

[14] Castanier, M., and Pierre, C., 2002. "Using intentional mistuning in the design of turbomachinery rotors". *AIAA Journal,* ***40***(10), pp. 2077–2086.

[15] Choi, B.-K., Lentz, J., Rivas-Guerra, A., and Mignolet, M., 2003. "Optimization of intentional mistuning patterns for the reduction of the forced response effects of unintentional mistuning: Formulation and assessment". *Journal of Engineering for Gas Turbines and Power,* ***125***(1), pp. 131–140.

[16] Mbaye, M., Soize, C., Ousty, J., and Capiez-Lernout, E., 2013. "Robust analysis of design in vibration of turbomachines". *Journal of Turbomachinery,* ***135***(2).

[17] Krack, M., Panning-Von Scheidt, L., Wallaschek, J., Siewert, C., and Hartung, A., 2013. "Reduced order modeling based on complex nonlinear modal analysis and its application to bladed disks with shroud contact". *Journal of Engineering for Gas Turbines and Power,* ***135***(10).

[18] Petrov, E., 2011. "A high-accuracy model reduction for analysis of nonlinear vibrations in structures with contact interfaces". *Journal of Engineering for Gas Turbines and Power,* ***133***(10).

[19] Capiez-Lernout, E., Soize, C., and Mignolet, M.-P., 2013. ""nonlinear stochastic dynamics for post-buckling analysis of uncertain cylindrical shells"". In Proceedings of the International Conference on Recent Advances in Structural Dynamics, RASD 2013, Pisa, Italy.

[20] Mignolet, M. P., Przekop, A., Rizzi, S. A., and Spottswood, S. M., 2013. "A review of indirect/non-intrusive reduced order modeling of nonlinear geometric structures". *Journal of Sound and Vibration,* ***332***(10), MAY 13, pp. 2437–2460.

[21] Muryavov, A., and Rizzi, S., 2003. "Determination of nonlinear stiffness with application to random vibration of geometrically nonlinear structures". *Computers & Structures,* ***81***, pp. 1513–1523.

[22] Mignolet, M.-P., and Soize, C., 2008. "Stochastic reduced order models for uncertain geometrically nonlinear dynamical systems". *Computer Methods in Applied Mechanics and Engineering,* ***197***, pp. 3951–3963.

[23] Capiez-Lernout, E., Soize, C., and Mignolet, M.-P., 2012. "Computational stochastic statics of an uncertain curved structure with geometrical nonlinearity in three-dimensional elasticity.". *Computational Mechanics,* ***49***(1), pp. 87–97.

[24] Soize, C., 2000. "A nonparametric model of random uncertainties for reduced matrix models in structural dynamics". *Probabilistic Engineering Mechanics,* ***15***(3), pp. 277–294.

[25] Soize, C., 2012. *Stochastic Models of Uncertainties in Computational Mechanics, Lecture Notes in Engineering Mechanics 2*. American Society of Civil Engineers (ASCE).

[26] Desceliers, C., and Soize, C., 2004. "Nonlinear viscoelastodynamic equations of three-dimensional rotating structures in finite displacement and finite element discretization". *International Journal of Nonlinear Mechanics,* ***39***, pp. 343–368.

[27] Davis, P., 1979. *Circulant matrices*. John Wiley & Sons.

[28] Mbaye, M., Soize, C., and Ousty, J.-P., 2010. "A reduced-order model of detuned cyclic dynamical systems with geometric modifications using a basis of cyclic modes". *ASME Journal of Engineering for Gas Turbines and Power,* ***132***(11).

[29] Crisfield, M., 1997. *Non-linear finite element analysis of solids and structures, Vol. 1 : essentials*. John Wiley and Sons, Chichester.

[30] Thomas, D., 1979. "Dynamics of rotationnally periodic structures". *International Journal for Numerical Methods in Engineering,* ***14***, pp. 81–102.

[31] Bossavit, A., 1993. "Boundary value problems with symmetry and their approximation by finite elements". *SIAM,* ***53***(5), pp. 1352–1380.

[32] Soize, C., 1982. "Medium frequency linear vibrations of anisotropic elastic structures.". *La recherche aérospatiale*, ***5***, pp. 65–87.
[33] Bowman, A. W., and Azzalini, A., 1997. *Smoothing Techniques for Data Analysis*. Oxford University Press.